Structure and Magnetic Properties of Regenerated Cellulose/Fe_3O_4 Nanocomposite Films

Jinping Zhou,[1,2] Ran Li,[1] Shilin Liu,[1] Qian Li,[1] Linzhi Zhang,[1] Lina Zhang,[1] Jianguo Guan[3]

[1]*Department of Chemistry, Wuhan University, Wuhan 430072, China*
[2]*Center of Nanoscience and Nanotechnology, Wuhan University, Wuhan 430072, China*
[3]*State Key Laboratory of Advanced Technology for Materials Synthesis and Processing, Wuhan University of Technology, Wuhan 430070, China*

Received 26 January 2008; accepted 27 July 2008
DOI 10.1002/app.29236
Published online 25 November 2008 in Wiley InterScience (www.interscience.wiley.com).

ABSTRACT: Cellulose nanocomposites containing high contents of Fe_3O_4 nanoparticles were successfully prepared with regenerated cellulose films as a matrix and mixture solutions of Fe^{2+}/Fe^{3+} as precursors. The structure and properties of the magnetic nanocomposite films were investigated with X-ray diffraction, scanning electron microscopy, transmission electron microscopy, thermogravimetric analysis, and vibrating sample magnetometry. Fe_3O_4 nanoparticles as prepared were irregular spheres and were homogeneously dispersed in the cellulose matrix. With an increase in the concentration of precursors from 0.2 to 1.0 mol/L, the content of Fe_3O_4 nanoparticles in the dried nanocomposites increased from 12 to 39 wt %, and the particle diameter increased from 32 to 64 nm. The cellulose nanocomposite films demonstrated superparamagnetic behavior, and their saturation magnetizations were in the range 4.2–21.2 emu/g, which were related to the increase in Fe_3O_4 nanoparticle content. With increasing nanophase content, the nanocomposite films displayed significantly anisotropic magnetic properties in the parallel and perpendicular directions. This study provided a green and facile method for the preparation of biobased nanocomposite films with high nanophase content and excellent magnetic properties. © 2008 Wiley Periodicals, Inc. J Appl Polym Sci 111: 2477–2484, 2009

Key words: film; nanocomposites; structure

INTRODUCTION

Polymer-based nanocomposites have attracted increasing attention over the last 2 decades because of their synergistic and hybrid properties derived from their individual components.[1–4] Biobased nanocomposites represent a new concept of ecological, bioinspired, and functional hybrid materials that are formed by the combination of natural polymers and inorganic solids and show at least one dimension at the nanometer scale.[5,6] These biohybrid materials not only display the improved structural and functional properties of conventional nanocomposites derived from synthetic polymers but also show the remarkable advantage of exhibiting biocompatibility, biodegradability, and some functional properties provided by either the biological or inorganic moieties.[7–10]

Cellulose, as a fascinating biopolymer and sustainable raw material, can be regenerated or derivatized to yield various useful products as a result of its renewability, biodegradability, and derivatizability.[11] Nanocomposites of cellulose and its derivatives are gaining importance because of their value-added applications in science and technology. Magnetic nanocomposites have been be prepared with swollen cellulosic materials such as wet-spun cellulose filaments and bacterial cellulose by *in situ* precipitation.[12–14] Cellulose acetate films containing iron or copper nanoparticles have been prepared by the mixture of iron or copper complexes and cellulose acetate in tetrahydrofuran followed by the casting of the mixture and the reduction of the metal complexes to nanoparticles.[15,16] Antimicrobial ultrafine cellulose acetate fibers with silver nanoparticles were prepared by the electrospinning of cellulose acetate solution with small amounts of silver nitrate followed by photoreduction.[17] Biodegradable nanocomposites were fabricated from cellulose acetate, ecofriendly triethyl citrate plasticizer, and organically modified clay by extrusion–injection processing.[18–20] More recently, Zhang et al.[21] prepared regenerated cellulose (RC)/multiwalled carbon nanotube composite fibers with enhanced mechanical properties and thermal stability in ionic liquid 1-allyl-3-methylimidazolium chloride. However, hybrid RC nanocomposite films or fibers have still not been well reported[22,23] because cellulose cannot be dissolved in common solvents on account of its strong intermolecular and intramolecular hydrogen bonds.

Correspondence to: J. Zhou (zhoujp325@whu.edu.cn).
Contract grant sponsor: National Natural Science Foundation of China; contract grant number: 20674057.

In our previous studies,[24,25] we developed a "green" solvent for cellulose, namely, NaOH/urea aqueous solution, and RC films and fibers with excellent mechanical properties have successfully been prepared.[26–28] The excellent mechanical properties, microporous structure, and chemical stability and remarkable hydrophilic properties of the cellulose films makes them suitable bulks for the fabrication of biobased nanocomposites. In this study, we attempted to provide a simple and green method to prepare cellulose/Fe_3O_4 nanocomposite films with high nanophase contents and excellent magnetic properties. Microporous RC films prepared in NaOH/urea aqueous solutions were used as nanoreactors, and the mixtures of aqueous solutions of Fe^{2+} and Fe^{3+} (molar ratio = 1 : 2) were used as precursors. The structure and properties of the nanocomposites were characterized with X-ray diffraction (XRD), scanning electron microscopy (SEM), transmission electron microscopy (TEM), thermogravimetric analysis (TGA), and vibrating sample magnetometry.

EXPERIMENTAL

Materials

Cellulose (cotton linter pulp) was supplied by Hubei Chemical Fiber Group, Ltd. (Xiangfan, China), and the viscosity-average molecular weight of the cellulose was determined by viscometry in cadoxen[29] to be 10.3×10^4. Ferric chloride ($FeCl_3 \cdot 6H_2O$), ferrous chloride ($FeCl_2 \cdot 4H_2O$), NaOH, urea, and sulfuric acid were analytical grade and were used without further purification.

Preparation of the films

Cellulose was dissolved directly in the NaOH/urea aqueous solution, which was precooled to −12°C, to prepare a transparent 4 wt % cellulose solution according to our previous method.[27] The resulting solution was centrifuged at 133.33 Hz for 20 min at 15°C for degasification. The cellulose solution was cast onto a glass plate to give a thickness of 0.5 mm and was then immersed in a 2000-mL H_2SO_4 (5 wt %) bath for 5 min for the coagulation and regeneration of the cellulose films. The resulting RC films were washed with running water and subsequently with distilled water.

The wet RC films (20×15 cm^2) obtained were immersed in a 500-mL mixture of aqueous $FeCl_2$ and $FeCl_3$ (molar ratio = 1 : 2) for 12 h; we then washed out the iron ions adsorbed on the surface of the film with distilled water. Then, the films were immersed in 500-mL of aqueous NaOH (4 mol/L) for 20 min and were then rinsed with distilled water for several times. The composite film containing iron oxides was fixed onto a plate of poly(methyl methacrylate) and air-dried at ambient conditions. The thickness of the composite films decreased to about 30–50 μm after drying, and there no shrinking occurred after the tension was released. By changing the concentration of the aqueous Fe^{2+}/Fe^{3+} solutions to 0.2, 0.4, 0.5, 0.6, 0.8, and 1.0 mol/L, we prepared a series of RC/Fe_3O_4 nanocomposite films and coded them as Fe02, Fe04, Fe05, Fe06, Fe08, and Fe10, respectively.

Characterization

SEM images of the films and nanoparticles were taken on a Sirion 200 field emission scanning electron microscope (FEI Co., Eindhoven, The Netherlands) at an accelerating voltage of 10 kV. RC and nanocomposite films in the wet state were frozen in liquid nitrogen, snapped immediately, and freeze-dried with a lyophilizer (Christ Alpha 1-2, Wertheim, Germany). Nanoparticles and the cross section of the films were sputtered with gold for SEM measurement. TEM and high-resolution transmission electron microscopy (HRTEM) images were taken on a JEM 2010 FEF (UHR) (JEOL Ltd., Tokyo, Japan) at 200 kV. The nanocomposite films were embedded in an epoxy resin. Ultrathin slices for TEM and HRTEM measurements were obtained via sectioning on an LKB-V ultratome (LKB, Bromma, Sweden).

XRD measurement was carried out on an X-ray diffractometer (D8, BRUKER AXS GmbH, Karlsruhe, Germany). An XRD pattern with Cu Kα radiation (1.5406×10^{-10} m) at 40 kV and 30 mA was recorded in the range $2\theta = 6$–80° at a scanning speed of 2°/min. TGA of the films was carried out with a thermal analyzer (STA 499C, Netzsch Co., Selb, Germany); the heating rate was 10°C/min from room temperature to 800°C under air atmosphere.

A vibrating sample magnetometer (AOEMODEL 4HF VSM, ADE, Ltd., Co., Westwood, MA, USA) was used to measure the magnetic properties of the nanocomposite films at room temperature. Hysteresis measurements were recorded with a static magnetic field applied first parallel and then perpendicular to the film. The applied field was systematically varied from −1.7 to 1.7 T.

RESULTS AND DISCUSSION

Structure and morphology of the films

The SEM image of the cross section of the freeze-dried RC film prepared from the NaOH/urea aqueous solutions is shown in Figure 1(a). The film displayed a homogeneous microporous structure in the inner section, and the mean pore size was calculated

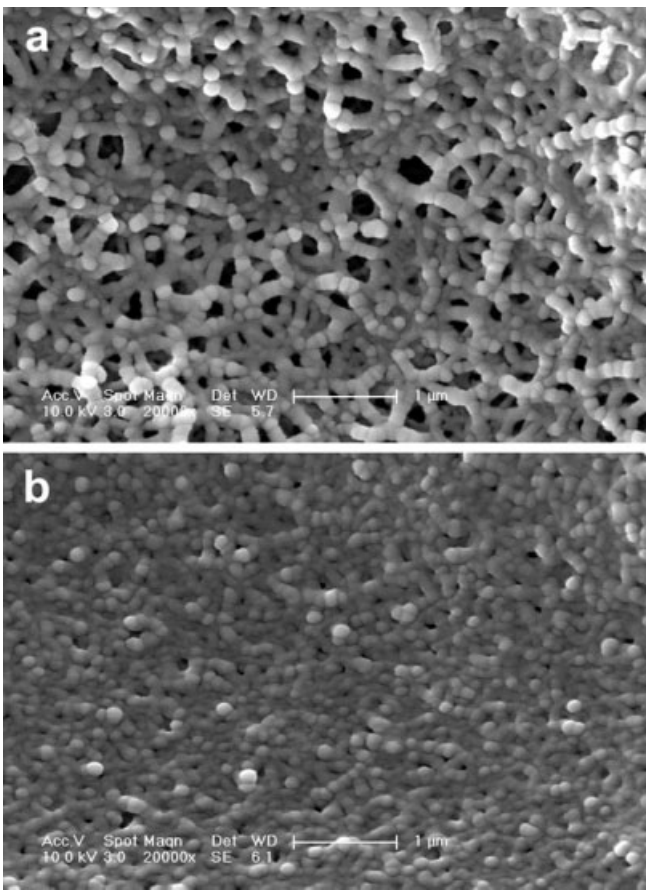

Figure 1 SEM images of cross sections of (a) the RC film and (b) nanocomposite film Fe05 by freeze drying.

to be about 180 nm. The porosity of the RC film was 88 vol % as determined by membrane osmometry.[27] As the RC films were immersed into a mixture of aqueous ferrous chloride ($FeCl_2$) and ferric chloride ($FeCl_3$), the iron ions were effectively diffused and adsorbed into the micropores of the films, which connected to the hydroxyl groups of cellulose by hydrogen bonds and other coordinating bonds.[30,31] When the films with adsorbed iron ions were immersed into the NaOH solution, the basic hydrolysis of the iron ions led to the formation of an iron oxide nanoparticle colloidal solution, and the films turned darker because of the formation of Fe_3O_4 nanoparticles. Figure 1(b) displays the SEM image of a cross section of the freeze-dried nanocomposite film (Fe05). The microporous structure of the pristine RC films [Fig. 1(a)] almost disappeared, which indicated that the Fe_3O_4 nanoparticles were *in situ* coprecipitated in the micropores of the cellulose matrix. Because there was a strong interaction between the nanoparticles and the cellulose matrix, the Fe_3O_4 nanoparticles dispersed in the film were stable and were hardly removed by washing with a large amount of water.

Figure 2 shows the powder XRD pattern of RC and the nanocomposite films. The diffraction peaks at $2\theta = 12$, 20, and 22° were assigned to the $(1\bar{1}0)$, (110), and (200) planes of the cellulose II crystalline form.[32] The crystallinity of cellulose in the nanocomposite films was apparently lower than that of the pure RC film and decreased with increasing of the content of Fe_3O_4 nanoparticles. The results indicate that the crystallinity of cellulose in the nanocomposites was partly destroyed because of the formation of nanoparticles. Except for the diffraction peaks of crystal cellulose II, the nanocomposite films displayed distinct peaks at 2θ values of 18.3, 30.4, 35.6, 43.5, 57.2, and 63.0, which corresponded to the characteristic peaks of Fe_3O_4 (Powder Diffraction file, JCPDS card no. 85-1436). Therefore, magnetic Fe_3O_4 nanoparticles were successfully synthesized in the

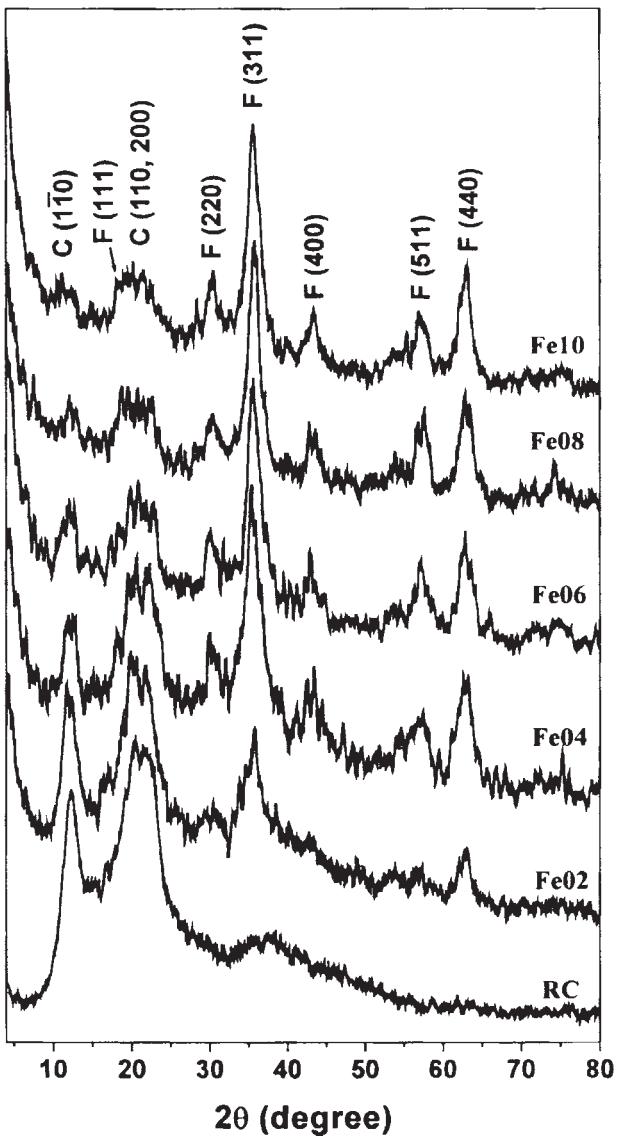

Figure 2 XRD patterns of the RC and nanocomposite films.

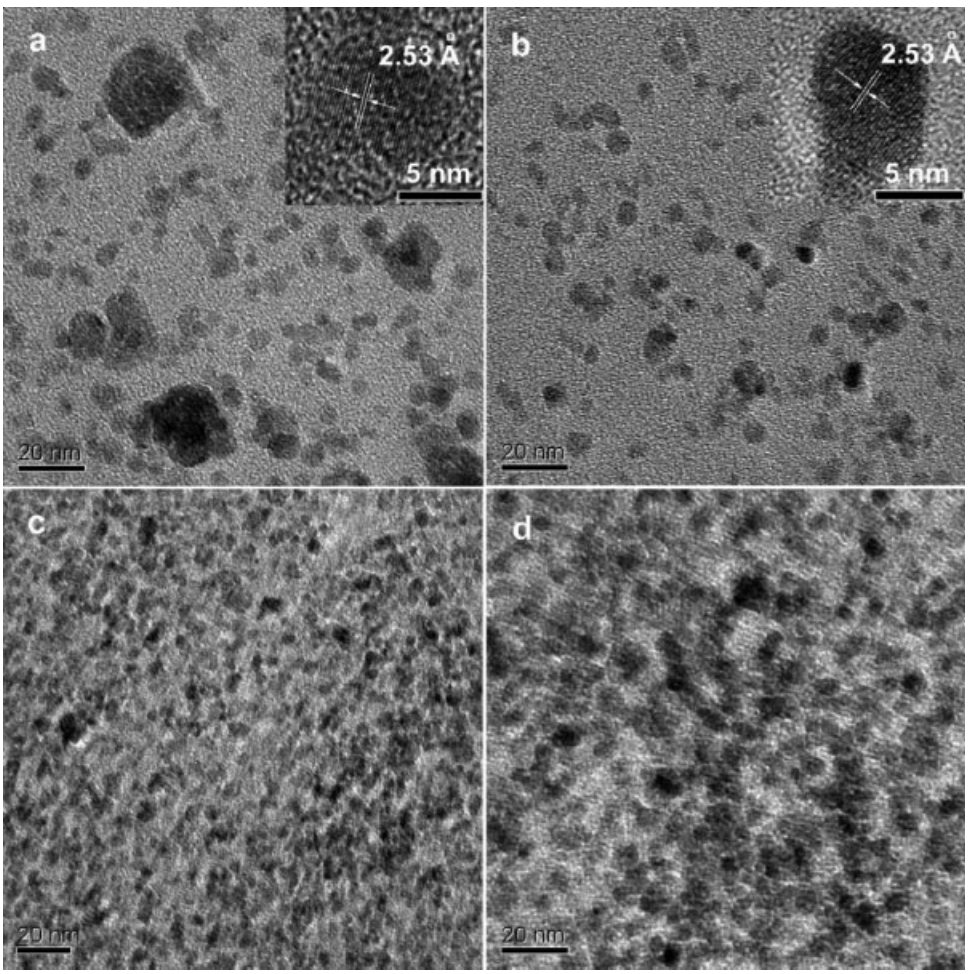

Figure 3 TEM images of (a,b) freeze-dried and (c,d) air-dried nanocomposite film Fe05: (a,c) ultrathin slices that parallel the film plane and (b,d) ultrathin slices that are perpendicular to the film plane. The insets of panels a and b are HRTEM images of the nanocomposite films.

micropores of the cellulose films by the coprecipitation of Fe^{2+} and Fe^{3+} ions. The relative intensity of the diffraction for magnetite nanoparticles increased with increasing concentration of precursors, which indicated an increase of nanophase loading in the cellulose matrix.

The morphology of Fe_3O_4 nanoparticles in the nanocomposite films was investigated with TEM. Figure 3 shows the TEM images of the nanocomposites (Fe05) by freeze-drying [Fig. 3(a,b)] and air-drying [Fig. 3(c,d)] methods. As observed in the ultrathin slices that were parallel and perpendicular to the film plane, the circular shapes of the Fe_3O_4 nanoparticles were separated from each other and were homogeneously dispersed in the cellulose matrix. We concluded that the nanoparticles formed in the cellulose matrix were irregular spheres, which were rather different from the disklike Fe_2O_3 nanoparticles synthesized in the RC films with Fe^{2+} ions as precursors.[33] On the basis of the morphological features and abundant surface hydroxyl groups of natural cellulose fibers, Kunitake et al.[34] developed a facile method to synthesize noble metal nanoparticles less than 10 nm in diameter and with narrow size distribution with porous cellulose fibers as nanoreactors and particle stabilizers. Similarly, RC films with a homogeneous microporous structure served as unique nanoreactors, particle controllers, and stabilizers in this study. The nanoparticles displayed a more dense dispersion in the air-dried films than those of the freeze-dried nanocomposites because of the shrinkage of the film during drying. The inset of Figure 3(a,b) shows the HRTEM images of the nanocomposites. The nanoparticles exhibited good crystallinity, and the lattice fringe of 2.53 Å was in good agreement with the separation between the (311) lattice planes of Fe_3O_4.

Properties of the films

The thermogravimetry (TG) and differential thermogravimetry (DTG) curves of the films under air atmosphere are plotted in Figure 4. A small weight loss of 8–11% around 80°C was assigned to the

release of moisture from the samples. The pure RC film showed two steps of active weight loss with elevating temperature. The first obvious weight loss was found in the temperature range 300–380°C, which was attributed to the onset of cellulose decomposition. The second weight loss peak at 420–540°C was caused by the oxidation and burning of cellulose. The thermal stability of the nanocomposites apparently decreased because of the destruction of the crystallinity of cellulose and the catalytic properties of the nanoparticles by the incorporation of Fe_3O_4 nanoparticles. With an increase in the nanophase content, the first weight loss stage of the nanocomposites shifted to lower temperatures. For example, the peak temperature of the first weight loss stage for the pure RC film was around 326°C, which decreased to 298°C when the nanophase content increased to 39 wt %. The second weight loss stages of the nanocomposites shifted to temperatures lower than 440°C and became a shoulder peak of the first weight loss stage.

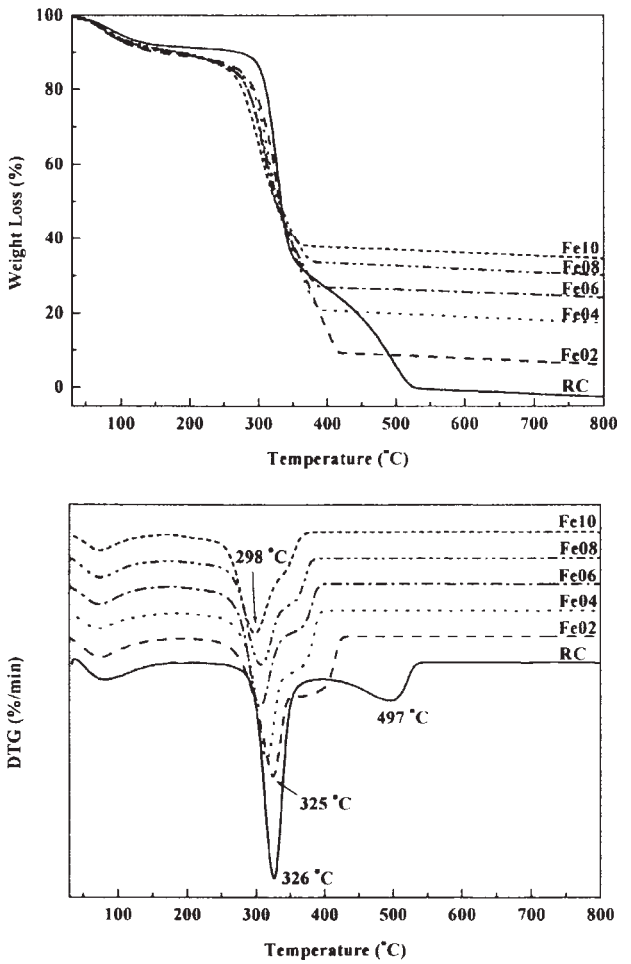

Figure 4 TG and DTG curves of the films under an air atmosphere. The DTG curves were vertically shifted for comparison.

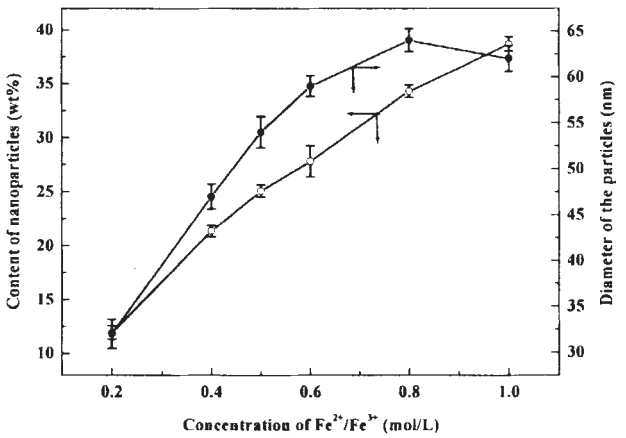

Figure 5 (○) Content and (●) diameter of the nanoparticles in the nanocomposite films as a function of the concentration of an aqueous Fe^{2+}/Fe^{3+} solution.

As determined by TGA (Fig. 4), the decomposition and burning temperature of cellulose in the nanocomposites ranged from 300 to 400°C. The RC/Fe_3O_4 nanocomposite films (ca. 2.0 g) were calcined in an oven at 450°C under an air atmosphere. As a result, the cellulose matrix burned out, and high-purity iron oxide nanoparticles were left behind. The content of Fe_3O_4 nanoparticles in the dried films as a function of the precursors concentration is plotted in Figure 5. With the concentration of Fe^{2+}/Fe^{3+} increased from 0.2 to 1.0 mol/L, the nanophase content increased from 12 to 39 wt %, which agreed well with the residue contents of the films determined by TGA. The high nanophase content in the cellulose matrix was attributed to the excellent hydrophilicity, abundance of microporous structure, and high porosity of the RC films. Figure 6 displays the SEM images of the nanoparticles after the calcinations of the nanocomposite films at 450°C under an air atmosphere. The diameter of the nanoparticles calculated from SEM images as a function of the concentration of precursors is also shown in Figure 5. The mean diameter of the particles increased linearly from 32 to 59 nm when the Fe^{2+}/Fe^{3+} concentration increased from 0.2 to 0.6 mol/L. When the concentration of precursors was further increased to 1.0 mol/L, the size of the nanoparticles increased slightly. The mean diameters of the nanoparticles were 64 and 62 nm at precursor concentrations of 0.8 and 1.0 mol/L, respectively. The microporous structure and abundance of —OH groups of the cellulose matrix played an important role in the growing and stabilization of the Fe_3O_4 nanoparticles and prevented the growth of larger particles from agglomeration. Therefore, this study provided a facile and green method for preparing nanocomposites with high nanophase contents and metal oxide nanoparticles with uniform size.

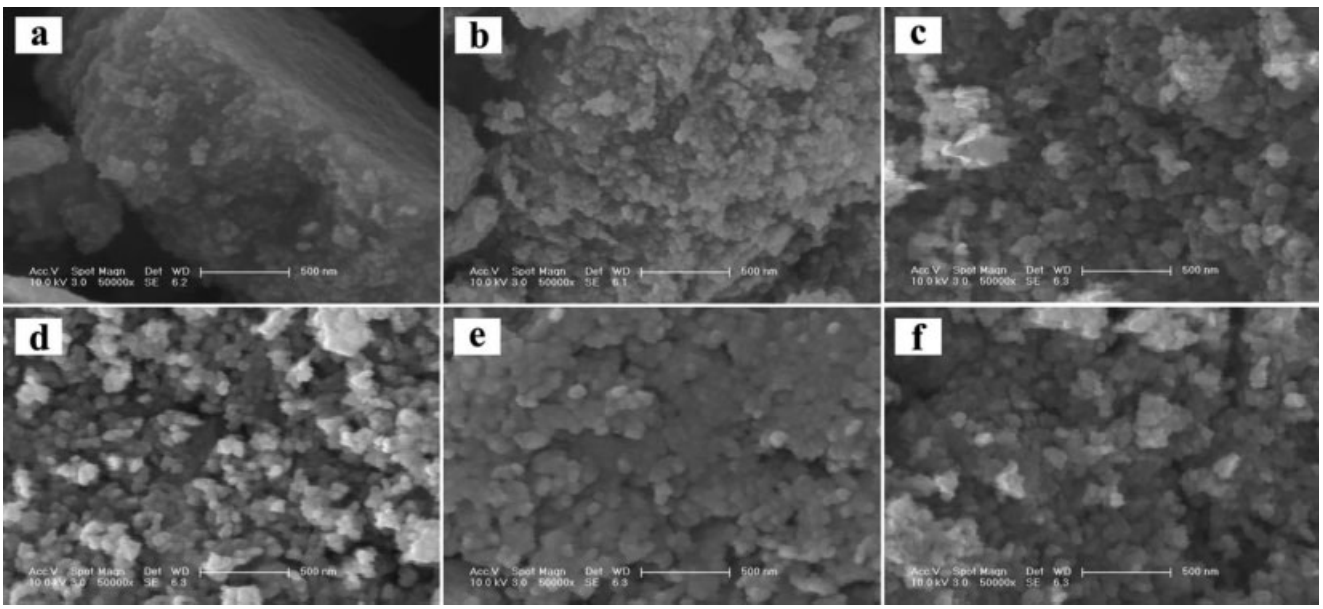

Figure 6 SEM images of the iron oxide nanoparticles after calcination of the nanocomposite films at 450°C under an air atmosphere: (a) Fe02, (b) Fe04, (c) Fe05, (d) Fe06, (e) Fe08, and (f) Fe10.

Magnetic properties

Figure 7 shows the magnetic hysteresis curves of the cellulose nanocomposite films measured at room temperature. All of the nanocomposite films exhibited superparamagnetic behavior with extremely small hysteresis loops and coercivity both in the parallel and perpendicularly applied fields. The lack of hysteresis and coercivity is characteristic of superparamagnetic particles and some single-domain particles.[35,36] The diameters of the magnetic nanoparticles synthesized *in situ* in the cellulose bulks were smaller than or around the critical size (54 nm) of the Fe_3O_4 single domains.[37] It has been known that magnetic particles smaller than some critical particle diameter can be called *single domains*. As the particles size continues to decrease below the single domain value, particles exhibit superparamagnetic properties, that is, no hysteresis and coercivity.[36]

The saturation magnetization (M_s) of the nanocomposite films as a function of the concentration of precursors is plotted in Figure 8. The M_s values of the nanocomposite films were in the range 4.2–21.2 emu/g, which were related to the increase in the Fe_3O_4 nanoparticle content. When the concentration of Fe^{2+}/Fe^{3+} solution was lower than 0.8 mol/L, the nanocomposites demonstrated isotropic magnetic properties for the random alignment of the easy magnetic axes, and their M_s values in the parallel and perpendicularly applied fields increased linearly with increasing concentration of precursors. Interestingly, the films displayed apparent magnetic anisotropy when the concentration of Fe^{2+}/Fe^{3+} solution was higher than 0.8 mol/L, and the M_s values in

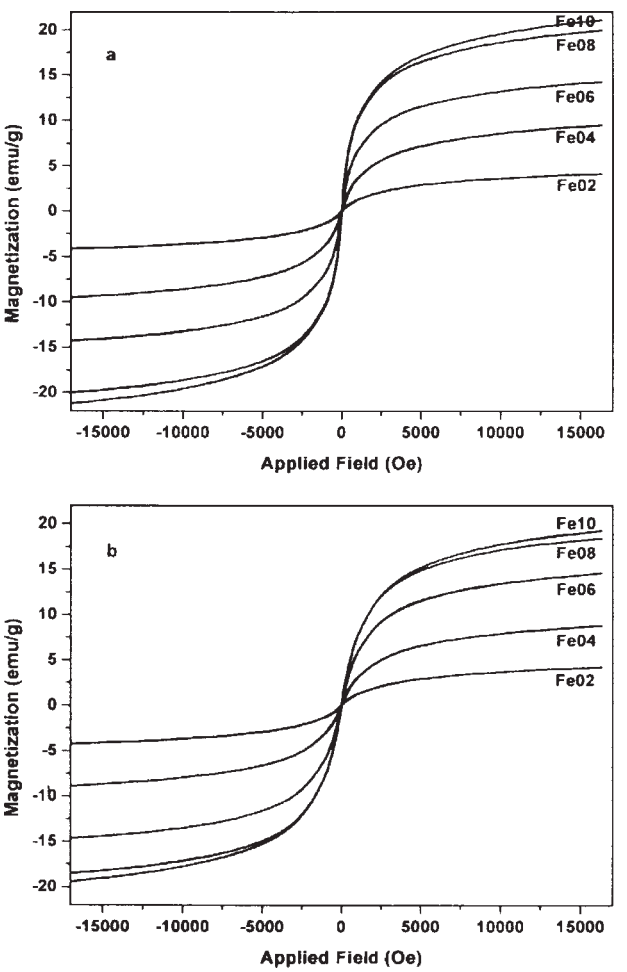

Figure 7 Hysteresis loops of the nanocomposite films measured at 298 K: (a) field parallel to the film and (b) field perpendicular to the film.

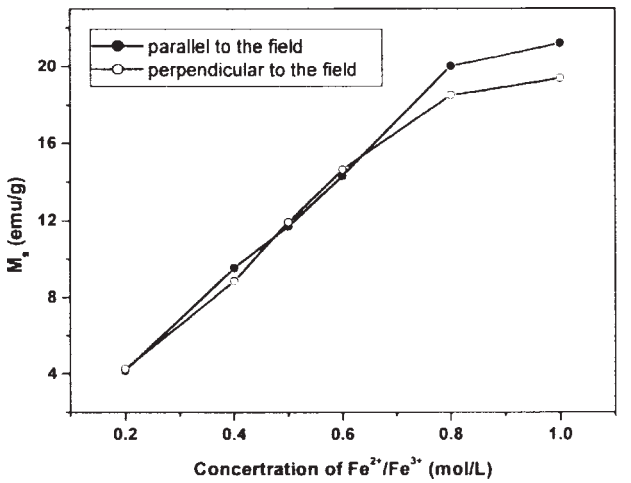

Figure 8 M_s of the nanocomposite films as a function of the concentration of an aqueous Fe^{2+}/Fe^{3+} solution. (●) field parallel to the film and (○) field perpendicular to the film.

parallel applied fields were significantly higher than those in perpendicularly applied fields. Kunitake et al.[34] reported that the magnetic anisotropy of composite film was achieved by the ordered orientation of magnetite particles in an ordered multibilayer film. We also prepared cellulose nanocomposite films with anisotropic magnetic properties via air-dried originates in the ordered alignment of iron oxide nanodisks.[33] Although the source of this anomaly in the high nanophase content was not clear, the strong dipole–dipole interaction between the magnetic nanoparticles inducing them form partly self-orientation of the easy magnetic axes in the cellulose matrix might have been a major reason. According to the nanophase content, the M_s values of the pure Fe_3O_4 nanoparticles were calculated. For the growth of particle size and enhancement in crystallinity, M_s of the pure Fe_3O_4 nanoparticles increased from 40 to 60 emu/g with an increase in the concentration of precursors. However, all of the calculated M_s values were smaller than their bulk values (92 emu/g for magnetite) because of the size effects of the nanoparticles. The RC nanocomposite films with interesting magnetic properties will find promising applications in many areas because magnetic polymer nanocomposites hold immense potential for application in cell separation, enzyme immunoassay, drug targeting, electromagnetic device applications, and electromagnetic interference suppression.[38–40]

CONCLUSIONS

We have described a green and facile method for the preparation of cellulose nanocomposite films containing high contents of Fe_3O_4 nanoparticles. The synthesized Fe_3O_4 nanoparticles were irregular spheres and were homogeneously dispersed in the cellulose matrix. With an increase in the concentration of aqueous Fe^{2+}/Fe^{3+} solutions from 0.2 to 1.0 mol/L, the Fe_3O_4 nanoparticle contents in the nanocomposites increased from 12 to 39 wt %, and the particle diameter increased from 32 to 64 nm. The crystallinity and thermal stability of cellulose decreased with the incorporation of Fe_3O_4 nanoparticles. The cellulose nanocomposite films demonstrated superparamagnetic behavior, and their M_s values increased from 4.2 to 21.2 emu/g with an increase in the Fe_3O_4 nanoparticle content. Moreover, the nanocomposites with high nanophase contents displayed significantly anisotropic magnetic properties in the parallel and perpendicular directions.

References

1. Gangopadhyay, R.; De, A. Chem Mater 2000, 12, 608.
2. Schmidt, G.; Malwitz, M. M. Curr Opin Colloid Interface Sci 2003, 8, 103.
3. Mark, J. E. Acc Chem Res 2006, 39, 881.
4. Vaia, R. A.; Maguire, J. F. Chem Mater 2007, 19, 2736.
5. Darder, M.; Aranda, P.; Ruiz-Hitzky, E. Adv Mater 2007, 19, 1309.
6. Yu, L.; Dean, K.; Li, L. Prog Polym Sci 2006, 31, 376.
7. Huang, M.; Yu, J.; Ma, X. Polymer 2004, 45, 7017.
8. Darder, M.; López-Blanco, M.; Aranda, P.; Aznar, A. J.; Bravo, J.; Ruiz-Hitzky, E. Chem Mater 2006, 18, 1602.
9. Chen, P.; Zhang, L. Biomacromolecules 2006, 7, 1700.
10. Sreedhar, B.; Aparna, Y.; Sairam, M.; Hebalkar, N. J Appl Polym Sci 2007, 105, 928.
11. Klemm, D.; Heublein, B.; Fink, H.-P.; Bohn, A. Angew Chem Int Ed 2005, 44, 3358.
12. Raymond, L.; Revol, J.-F.; Rayan, D. H.; Marchessault, R. H. Chem Mater 1994, 6, 249.
13. Raymond, L.; Revol, J.-F.; Marchessault, R. H.; Rayan, D. H. Polymer 1995, 36, 5035.
14. Sourty, E.; Ryan, D. H.; Marchessault, R. H. Chem Mater 1998, 10, 1755.
15. Shim, I. W.; Choi, S.; Noh, W. T.; Kwon, J.; Cho, J. Y.; Chae, D. Y.; Kim, K. S. Bull Korean Chem Soc 2001, 22, 772.
16. Shim, I. W.; Noh, W. T.; Kwon, J.; Cho, J. Y.; Kim, K. S.; Kang, D. H. Bull Korean Chem Soc 2002, 23, 563.
17. Son, W. K.; Youk, J. H.; Lee, T. S.; Park, W. H. Macromol Rapid Commun 2004, 25, 1632.
18. Park, H.-M.; Misra, M.; Drzal, L. T.; Mohanty, A. K. Biomacromolecules 2004, 5, 2281.
19. Park, H.-M.; Liang, X.; Mohanty, A. K.; Misra, M.; Drzal, L. T. Macromolecules 2004, 37, 9076.
20. Park, H.-M.; Mohanty, A. K.; Drzal, L. T.; Lee, E.; Mielewski, D. F.; Misra, M. J Polym Environ 2006, 14, 27.
21. Zhang, H.; Wang, Z.; Zhang, Z.; Wu, J.; Zhang, J.; He, J. Adv Mater 2007, 19, 698.
22. Zhou, J.; Liu, S.; Qi, J.; Zhang, L. J Appl Polym Sci 2006, 101, 3600.
23. Chang, J.-H.; Nam, S. W.; Jiang, S. W. J Appl Polym Sci 2007, 106, 2970.
24. Zhang, L.; Zhou, J. Chin. Pat. ZL00114486.3 (2003).
25. Zhang, L.; Cai, J.; Zhou, J. Chin. Pat. 03128386.1 (2005).
26. Zhou, J.; Zhang, L.; Cai, J.; Shu, H. J Membr Sci 2002, 210, 77.
27. Zhang, L.; Mao, Y.; Zhou, J.; Cai, J. Ind Eng Chem Res 2005, 44, 522.

28. Cai, J.; Zhang, L.; Zhou, J.; Qi, H.; Chen, H.; Kondo, T.; Chen, X.; Chu, B. Adv Mater 2007, 19, 821.
29. Brown, W.; Wiskstön, R. Eur Polym J 1965, 1, 1.
30. Huang, J.; Matsunaga, N.; Shimanoe, K.; Yamazoe, N.; Kunitake, T. Chem Mater 2005, 17, 3513.
31. Huang, J.; Ichinose, I.; Kunitake, T. Angew Chem Int Ed 2006, 45, 2883.
32. Marchessault, R.; Sundarajan, P. In The Polysaccharides; Aspinal, G., Ed.; Academic: New York, 1985; Vol. 2, p 11.
33. Liu, S.; Zhou, J.; Zhang, L.; Guan, J.; Wang, J. Macromol Rapid Commun 2006, 27, 2084.
34. He, J.; Kunitake, T.; Nakao, A. Chem Mater 2003, 15, 4401.
35. Leslie-Pelecky, D. L.; Rieke, R. D. Chem Mater 1996, 8, 1770.
36. Kim, J.-Y.; Shin, D.-H.; Ihn, K.-J.; Nam, C.-W. Macromol Chem Phys 2002, 203, 2454.
37. Aharoni, A.; Jakubovics, J. P. IEEE Trans Magn 1988, 24, 1892.
38. Zhang, L. J.; Wan, M. X. J Phys Chem B 2003, 107, 6748.
39. Dey, A.; De, S.; De, A.; De, S. K. Nanotechnology 2004, 15, 1277.
40. Alam, J.; Riaz, U.; Ahmad, S. J Magn Magn Mater 2007, 314, 93.